Biosensors and Bioelectronics 141 (2019) 111357

Contents lists available at ScienceDirect

Biosensors and Bioelectronics

journal homepage: www.elsevier.com/locate/bios

Development of highly sensitive IgA immunosensors based on co-electropolymerized L-DOPA/dopamine carbon nano-onion modified electrodes

Julio C. Zuaznabar-Gardona, Alex Fragoso*

Nanobiotechnology & Bioanalysis Group, Departament d' Enginyeria Química, Universitat Rovira i Virgili, Avinguda Països Catalans 26, 43007, Tarragona, Spain

ARTICLE INFO

Keywords:
Carbon nano-onions
L-DOPA
Dopamine
Immunoglobulin a
Electrochemical immunosensor
Aminoferrocene

ABSTRACT

The development of versatile platforms to construct novel and sensitive immunosensors is nowadays an intense research field. Nanomaterials and polymers are often combined to fabricate new platforms to immobilize capture antibodies. Here we evaluate for the first time the co-electropolymerization of dopamine (DA) and L-3,4-dihydroxyphenylalanine (L-DOPA) on carbon nano-onion (CNO) modified electrodes as versatile platform to develop electrochemical immunosensors. Mixtures of DA and L-DOPA at different molar rations were co-electropolymerized on CNO-modified glassy carbon electrodes to form a poly(L-DOPA/DA) film. Immobilization of aminoferrocene was used to estimate the number of accessible carboxylic acid groups on the surface (11.3 nmol/cm^2), a value comparable to three-dimensional matrices. This platform was applied to the electrochemical detection of IgA antibodies using both a HRP-based sandwich type assay and label-free detection based on $[Fe(CN)_6]^{3-/4-}$ signal blocking. The sandwich and the label-free assays showed a wide linear response with LOD of 19 and 48 ng/mL, respectively, allowing the detection of serum IgA deficiency. Most remarkably, the incorporation of CNO layer led to a significant improvement (three-orders of magnitude) of the analytical performance of these immunosensors due to a combination of high surface area and increased electron transfer rates provided by the CNO layer.

1. Introduction

Immunoassays are undoubtedly useful analytical tools in today medical diagnosis and biochemical analysis. They are based on the specific affinity between an antibody and its corresponding antigen (e.g. antibodies, proteins, hormones, viruses, toxins, etc.) (Wild, 2013). Various assay formats have been developed such as enzyme-linked immunoassay (Leonardo et al., 2018), radioimmunoassay (Goldsmith, 1975), time-resolved fluorescence (Diamandis and Christopoulos, 1990), flow injection (Krämer and Schmid, 1991), quartz crystal microbalance (Zhang et al., 2017), surface plasmon resonance (Wu et al., 2015) and lateral flow (Bahadır and Sezgintürk, 2016a). Among them, the enzyme-linked immunosorbent assays (ELISA) and lateral flow immunoassays are the most popular and widely used in research and medical laboratories.

In recent years, electrochemical immunoassays have attracted great interest among industry and academy (Kokkinos et al., 2016). Their working principle relies on monitoring the specific recognition event between the capture antibody and its antigen by using an electrochemical technique (Piro et al., 2017). Different reviews have summarized the practical aspects (Ricci et al., 2012) and the various available architectures and transduction strategies to develop electrochemical immunoassays (Kokkinos et al., 2016). They are of particular interest given the combination of specificity and selectivity of the immunoreaction with the sensitivity, short response times, low cost of instrumentation and possibility of lab decentralization offered by electrochemical techniques (Pakchin et al., 2017).

Nanomaterials have been successfully applied to develop novel and sensitive electrochemical immunoassays (Valera et al., 2016). Noble metal nanoparticles, chalcogenides, metal oxide nanoparticles and carbon-based materials could be used as platform for attaching the capture probes as well as labels of the secondary antibody (Ortega et al., 2018). The incorporation of nanomaterials in electrochemical immunosensors results in an enhancement of the sensitivity and improvement of the limit of detection.

Carbon nanotubes and graphene are widely used as platforms to anchor biorecognition elements (Bahadır and Sezgintürk, 2016b; Sireesha et al., 2018). Carbon nano-onions (CNOs) were discovered in

* Corresponding author.
E-mail address: alex.fragoso@urv.cat (A. Fragoso).

https://doi.org/10.1016/j.bios.2019.111357
Received 9 March 2019; Received in revised form 9 April 2019; Accepted 26 May 2019
Available online 30 May 2019
0956-5663/

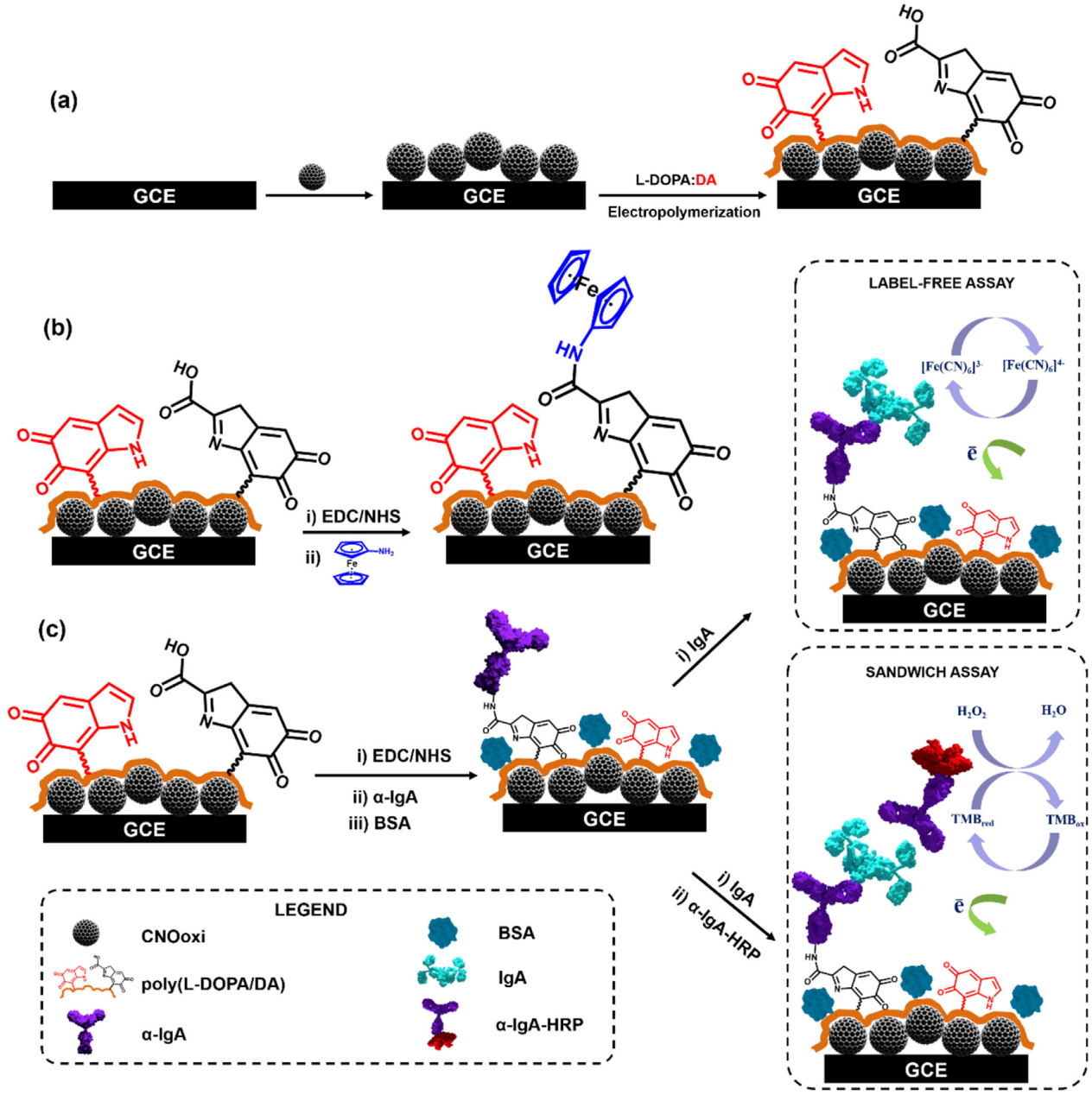

Scheme 1. Schematic representation of the steps involved in: (a) the modification of the GCE surfaces with CNOoxi and poly(L-DOPA/DA) film; (b) the attachment of aminoferrocene and (c) the construction of the two assay formats for the electrochemical detection of IgA antibodies.

the early 90's and consist of multilayered fullerenes concentrically arranged resembling the structure of an onion (Mykhailiv et al., 2017). Recent bioanalytical applications of CNOs include their incorporation on a polymeric composite and gold nanoparticles to detect human chorionic gonadotropin (Rizwan et al., 2019) and carcinoembryonic antigen (Rizwan et al., 2018a). As we have previously demonstrated, CNOs greatly improve biosensor sensitivity by a combination of enhanced surface area and electron transfer rate (Bartolome et al., 2015; Bartolome and Fragoso, 2017; Zuaznabar-Gardona and Fragoso, 2018).

An important aspect in the development of electrochemical immunoassays is the immobilization of the biorecognition elements on the electrode surface in a way that provides a large immunoreagent load with optimal orientation and spacing (Trilling et al., 2013). Polymeric films derived from catecholamines such as dopamine have recently been explored for the immobilization of a wide range of biomolecules (Liu et al., 2014; Barclay et al., 2017). Other catecholamines, such as 3-(3,4-dihydroxyphenyl)-L-alanine) (L-DOPA) which bears a carboxylic acid group has been rarely used for this purpose (Dai et al., 2015), while the copolymerization of catecholamine mixtures to anchor biomolecules has not been reported.

In this work, we explore the co-electropolymerization of L-DOPA and DA on glassy carbon electrodes covered with a film of oxidized CNOs (Scheme 1a) and apply it to construct a novel and sensitive electrochemical immunosensor for immunoglobulin A (IgA). IgA antibodies are the second most prevalent immunoglobulin in circulation and its deficiency is related with different immune diseases (Cruse and Lewis, 2010). Furthermore, IgA concentrations are an indication of overall body condition and, in pathological situations, may help in determining cancer staging and other diagnostic conditions (Soo-Quee Koh and Choon-Huat Koh, 2007).

2. Materials and methods

Dopamine hydrochloride (DA), 3-(3,4-dihydroxyphenyl)-L-alanine)

(L-DOPA), dimethylformamide (DMF), KCl, $K_4[Fe(CN)_6]$, $K_3[Fe(CN)_6]$, 1-ethyl-3-(3-dimethyl-aminopropyl) carbodiimide hydrochloride (EDC), N-hydroxysuccinimide (NHS), sodium acetate, acetic acid, sulfuric acid 97%, ethanolamine, 2-(N-morpholino)ethanesulfonic acid (MES), 3,3′,5,5′-tetramethylbenzidine (TMB), anti-human IgA (α-chain specific) antibody produced in goat (α-IgA), IgA from human colostrum, anti-human IgA-peroxidase (α-IgA-HRP), human IgG, human IgE, bovine serum albumin (BSA), calf serum and skim milk were obtained from Sigma–Aldrich and were used as received. Solutions were prepared with double distilled water (18.2 MΩ cm) obtained from a Milli-Q® system (Millipore, Madrid, Spain). CNOs were prepared and further oxidized as previously reported (Wajs et al., 2015). Phosphate-buffered saline (PBS) and PBS with 0.05% v/v Tween 20 were made from tablets purchased from Sigma–Aldrich. Phosphate buffers (PB, 0.01 mol/L) were prepared by mixing different volumes of 0.01 mol/L Na_2HPO_4 and 0.01 mol/L NaH_2PO_4 solutions. pH values were adjusted with 1 mol/L NaOH or 1 mol/L HCl.

All electrochemical measurements were obtained using a PC-controlled CHI 660A electrochemical workstation (CH Instruments, Austin, USA) with a three-electrode cell configuration. Glassy carbon electrodes (CH Instruments model CHI104, 3.0 mm diameter) coated with oxidized CNO films (GCE/CNOoxi) were used as working electrode. A platinum wire and Ag/AgCl(sat) were used as counter and reference electrodes, respectively.

2.1. Electrode preparation

Prior to modification, bare GCE electrodes were first manually smoothed with emery paper # 600 followed by polishing to a mirror finish with 0.3 μm alumina slurries. The polished GCE were sonicated in Milli-Q® water for 5 min and dried under a stream of nitrogen. GCE were modified by drop-casting a homogeneous dispersion of CNOoxi in DMF (4 mg/mL) prepared using an ultrasonic-bath for 30 min. To obtain a thin layer of CNOoxi, 1 μL of the dispersion was cast on the surface of the electrodes and dried in an oven at 80 °C for 2 h.

2.2. Electrochemical co-polymerization of catecholamines on GCE/CNOoxi

A poly(L-DOPA/DA) film was formed on the surface of GCE/CNOoxi electrodes by electrochemical polymerization of L-DOPA and DA mixtures (Scheme 1a). Briefly, GCE/CNOoxi electrodes were dipped in a solution containing different molar ratios of L-DOPA and DA in PB 0.01 mol/L pH 6.5. Then, 10 potential cycles were applied to the electrodes between −0.5 and 1.5 V at 100 mV/s. After that, the modified electrodes (denoted as GCE/CNOoxi/poly(L-DOPA/DA) were stabilized by cycling 20 times the potential between −0.2 and 0.9 V at 100 mV/s in PB 0.01 mol/L pH 6.5. Finally, the electrodes were thoroughly washed with Milli-Q® water, dried and stored at room temperature.

2.3. Aminoferrocene modified GCE/CNOoxi/poly(L-DOPA/DA)

GCE/CNOoxi/poly(L-DOPA/DA) electrodes were immersed in a stirring solution containing 5 mM of EDC and NHS in 0.1 M MES buffer pH 5 for 30 min to activate the COOH groups of the poly(L-DOPA/DA) films. Then, the electrodes were stirred for 1 h in 250 μM aminoferrocene ($FcNH_2$) solution in PBS containing 10% v/v DMSO (Scheme 1b). The modified electrodes were thoroughly washed with Milli-Q water, dried with N_2 and stored at room temperature.

2.4. IgA immunosensor

The carboxylic acid moieties of the GCE/CNOoxi/poly(L-DOPA/DA) were activated with EDC and NHS followed by immersion in 100 μg/mL α-IgA in PBS pH 7.4 for 1.5 h at room temperature followed by 1% BSA in PBS pH 7.4 for 30 min. After washing with PBS solution to remove unbound molecules, electrodes were dried and stored at 4 °C before being used.

2.4.1. Detection of IgA antibodies

Label-free assay: The immunosensors were incubated with 200 μL IgA target in PBS pH 7.4 at different concentrations for 1 h and rinsed with PBS. Differential pulse voltammograms were recorded between −0.2 and + 1 V (vs. Ag/AgCl reference electrode) in 1 mmol/L $[Fe(CN)_6]^{3-/4-}$ in PBS pH 7.4. A calibration curve was constructed from the change in the DPV peak current before and after the antigen-antibody reaction at different IgA concentrations.

Sandwich type assay: In this case, after the capture of IgA the immunosensors were incubated with HRP-labeled anti-human IgA (1:1000 dilution) for 15 min followed by rinsing with PBS. Amperometric measurements were carried out at 0.2 V in a 5 mL electrochemical cell containing TMB liquid substrate in 0.1 M PB pH 6 (1:10 v/v) under stirring conditions at room temperature. Current values *vs.* IgA concentration were used to obtain the calibration plots.

In all cases, control measurements were carried out with electrodes prepared in the absence of CNOs (GCE/poly(L-DOPA/DA).

2.5. Colorimetric detection of IgA

Nunc® 96-well polypropylene plates from Thermo Fisher Scientific (Madrid, Spain) were incubated overnight at 4 °C with 100 μL of 10 μg/mL α-IgA in carbonate buffer pH 9.6. After washing, the remaining active sites were blocked with 1% BSA in PBS at 37 °C for 1 h. After rinsing, 100 μL of IgA standards were added, incubated for 1 h and washed. Detection was carried out by addition of 100 μL of anti-human IgA HRP-conjugate (1:10 000 in PBS) for 15 min. After washing and incubation with 100 μL of TMB for 10 min, the reaction was stopped with 1 mol/L H_2SO_4 and the absorbance of each well was measured at 450 nm in a Wallac Victor2 1420 multiplate reader from Perkin-Elmer. The washing steps consisted in soaking four times the wells with 200 μL of PBS with 0.05% v/v Tween 20.

2.6. Analysis of spiked serum samples and stability study of GCE/CNOoxi/poly(L-DOPA/DA)/α − IgA

A calf serum sample was diluted with PBS pH 7.4 (1:100 v/v) and spiked with 70 and 1000 ng/mL of IgA and the current response was measured as described for the sandwich type assay. Recoveries were calculated by dividing the obtained currents with those expected from the corresponding calibration curve (Fig. 4b).

For the stability study, the biosensors were stored in StabilCoat® Plus Stabilizer (from Surmodics) for one week at 4 °C and 37 °C in order to test their stability in real time and under accelerated conditions. The sandwich assay was then constructed using 1000 ng/mL of IgA in PBS pH 7.4 and the current was measured and compared with the calibration curve.

All measurements were carried out in triplicate in three freshly prepared biosensors.

3. Results and discussion

3.1. Electrochemical copolymerization of L-DOPA and DA mixtures on GCE/CNOoxi

CNOoxi was prepared by nanodiamond annealing and acid oxidation and consist in ~5 nm nanoparticles with 5–6 graphitic layers (Fig. 1a). The GCE/CNOoxi electrodes were coated with a film of poly (L-DOPA/DA) by oxidative co-electropolymerization of a mixture of L-DOPA and DA in a buffer solution using cyclic voltammetry. The ESEM image of GCE/CNOoxi/poly(L-DOPA/DA) electrodes (Fig. 1b) show a markedly rough surface due to the CNOoxi layer. The presence of the poly(L-DOPA/DA) coating was confirmed by XPS (Fig. 1c and S1,

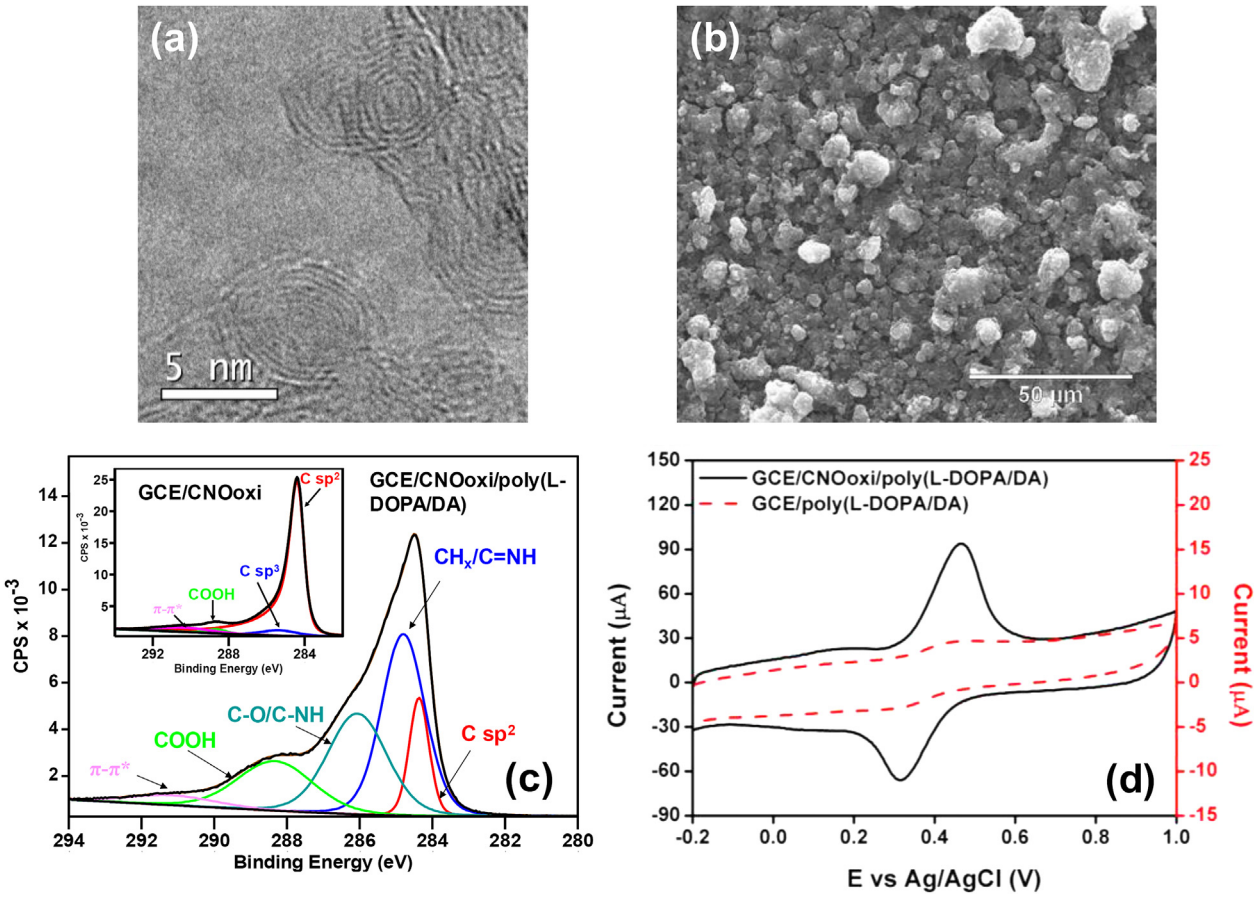

Fig. 1. a) HRTEM image of CNOoxi. b) ESEM image of the GCE/CNOoxi/poly(L-DOPA/DA) surface. c) High resolution XPS spectra in the C 1s region of GCE/CNOoxi/poly(L-DOPA/DA) and GCE/CNOoxi (inset). d) Cyclic voltammograms for poly(L-DOPA/DA)-modified electrodes in the absence and presence of CNOoxi in 0.1 mol/L acetate buffer pH 5.0. Scan rate is 0.1 V/s.

Supplementary Material). As can be seen from Fig. 1c, the C 1s region can be peak-fitted into five components corresponding to C sp^2 (284.4 eV, 11.6%), CHx/C=NH (284.8 eV, 39.3%), C–O/C–NH (286.1 eV, 27.7%), COOH (288.3 eV, 19.4%) and the π-π* relaxation shake-up (291.2 eV, 2%) (Clark et al., 1990). This spectrum markedly differs from that of GCE/CNOoxi, in which C sp^2 (284.3 eV, 88.2%) is the major peak.

Cyclic voltammograms of the first electropolymerization cycle in 10 mmol/L phosphate buffer pH 6.5 with 1:0, 1:5, 1:10, 1:20 and 0:1 L-DOPA:DA molar ratios are shown in Fig. S2 (Supplementary Material). The peaks in the voltammograms are related with the redox processes that take place during the oxidative electropolymerization of catecholamines. In general, the intensity of the current peaks decreased cycle by cycle indicating a gradual decrease in the electrode activity toward L-DOPA and DA due to the electropolymerization of L-DOPA and DA on the GCE/CNOoxi surface.

The modified GCE/CNOoxi/poly(L-DOPA/DA) electrodes display well-defined anodic and cathodic peaks centered at 0.40 V, assigned to a two-electron-two proton oxidation/reduction of quinone/hydroquinone moieties in the deposited film (Fig. 1d). The pH dependence of the oxidation-reduction peak potential was confirmed by recording cyclic voltammograms at different pH (Fig. S3 in Supplementary Material). Both peaks shifted to more negative potentials as pH was increased. This kind of pH-dependent redox behavior has been applied for voltammetry and potentiometric determinations of pH (Amiri et al., 2016; Zuaznabar-Gardona and Fragoso, 2018). The linearity observed between peak current and potential scan rates indicates that the quinone/hydroquinone redox conversion is surface confined, confirming the functionalization of the electrode surface with poly(L-DOPA/DA) films (Fig. S4 in Supplementary Material). Remarkably, the peak current intensities of GCE/CNOoxi/poly(L-DOPA/DA) were ~70-fold higher than those for GCE/poly(L-DOPA/DA) electrodes. This marked difference in current values can be explained considering that the CNOoxi increase the effective surface-active area of the electrodes and the presence of structural defects due to functionalization favor the electron-transfer kinetics (Borgohain et al., 2014; Bartolome et al., 2015). As a result, an enhancement of the current intensity of the electroactive species is observed when CNOoxi are incorporated as conductive layer on GCE surfaces.

Aminoferrocene ($FcNH_2$) was used to estimate the L-DOPA:DA ratio that results in a poly(L-DOPA/DA) film with the highest number of available carboxylic acid moieties by attaching $FcNH_2$ via carbodiimide chemistry (Scheme 1b). Cyclic voltammograms recorded in 0.1 mol/L $NaClO_4$ showed a pair of anodic and cathodic peaks assigned to the ferrocenium/ferrocene (Fc^+/Fc) redox couple (Fig. 2a) centered at +0.4 V. The current intensities were also much higher in the case of electrodes incorporating CNOoxi in comparison to GCE. The linear dependence of the current intensity with the scan rate indicates that the Fc^+/Fc redox couples was attached to the electrode surface (Fig. S5 in Supplementary Material). Increasing the L-DOPA:DA molar ratio leads to increased anodic peak currents with a maximum at 1:10 L-DOPA:DA molar ratio followed by a further current decrease as the L-DOPA:DA ratio increases. This is explained considering that the DA residues spatially separate the carboxylic acid groups in the electropolymerized film up to an optimal ratio after which reducing the steric hindrance hampers further reactions. The interfacial concentration of immobilized ferrocene for this composition was (11.3 ± 0.4) nmol/cm^2. This value is 4.7 times higher than that obtained for ferrocenehexanethiol

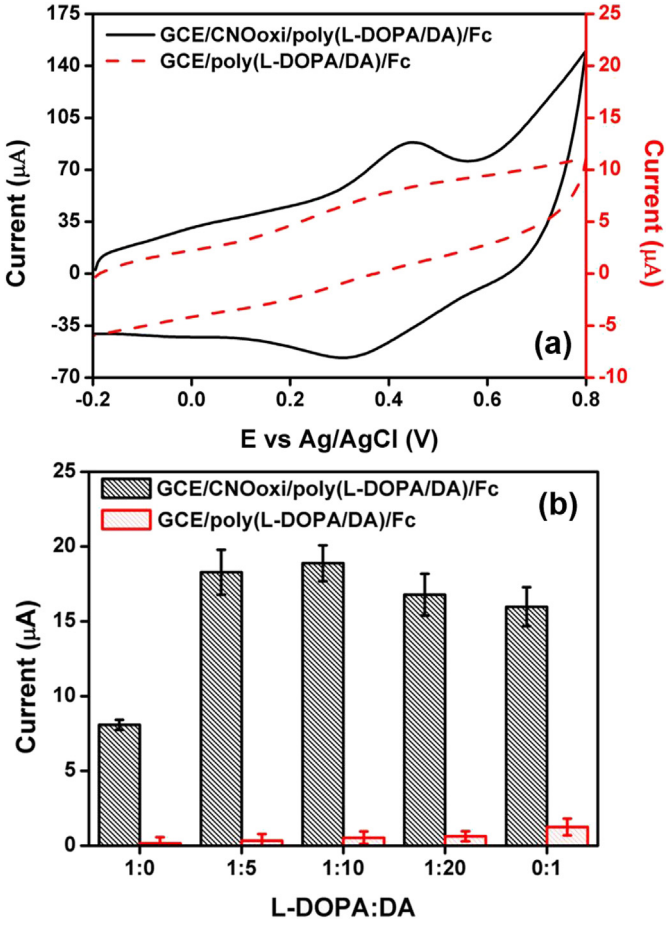

Fig. 2. (a) Cyclic voltammograms of GCE/CNOoxi/poly(L-DOPA/DA) and GCE/poly(L-DOPA/DA) after covalent attachment of aminoferrocene in 0.1 mol/L $NaClO_4$ at 0.1 V/s. (b) Plot of the anodic current of ferrocene-modified electrodes at different L-DOPA:DA ratios. All measurements were carried out in triplicate.

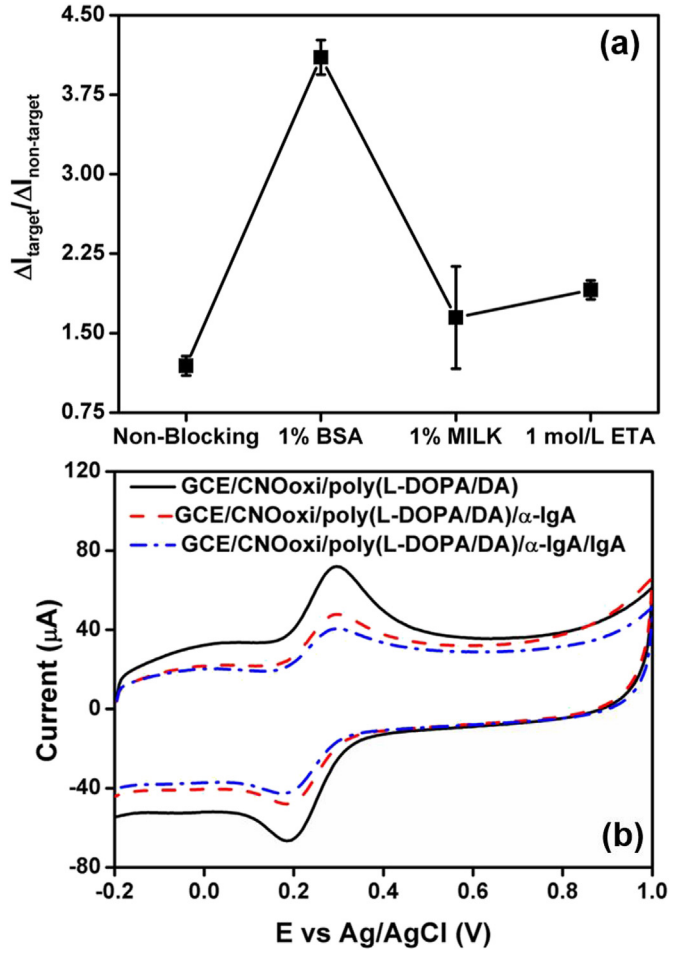

Fig. 3. (a) Effect of blocking agents on the DPV peak current of 1 mmol/L $[Fe(CN)_6]^{3-/4-}$ in PB before ($\Delta I_{non\text{-}target}$) and after ($\Delta I_{target}$) incubation with 500 ng/mL IgA on GCE/CNOoxi/poly(L-DOPA/DA)/α-IgA electrodes (BSA: bovine serum albumin, MILK: skim milk, ETA: ethanolamine). All measurements were carried out in triplicate. (b) Cyclic voltammograms for the steps involved in the construction of the IgA immunosensors in PBS containing 1 mmol/L $[Fe(CN)_6]^{3-/4-}$.

immobilized on a maleimide-CNO surface (Bartolome et al., 2015) and only 30% lower to that reported for Fc covalently grafted to a three-dimensional poly-aminoethylphenylene/MWCNT surface (Le Goff et al., 2010). This indicates that the surface resulting from the co-electropolymerization of the catecholamine mixture on the CNO surface contains a very large number of accessible carboxylate groups, at least for a small molecule like aminoferrocene. Thus, the 1:10 L-DOPA:DA ratio was used in the construction of the immunosensors.

3.2. Fabrication of the electrochemical immunosensors for IgA detection

The GCE/CNOoxi/poly(L-DOPA/DA) electrodes were used as a platform to construct a label-free and a sandwich type electrochemical immunoassay to detect IgA antibodies based on immobilized anti-human IgA antibodies (Scheme 1c).

Different blocking agents (1% BSA, 1% skim milk and 1 mol/L ethanolamine) were initially tested in order to minimize non-specific adsorption. The influence of the tested blocking agents on the signal response of the immunosensor in presence of $[Fe(CN)_6]^{3-/4-}$ before and after incubation of 500 ng/mL IgA is shown in Fig. 3a. It is observed that the largest target/non-target current ratio was measured when 1% BSA was used and was thus selected as blocking agent for further work. Fig. 3b shows the cyclic voltammograms in $[Fe(CN)_6]^{3-/4-}$ of the sequential steps leading to the preparation of the biosensor and after interaction with IgA. The CV of the GCE/CNOoxi/poly(L-DOPA/DA) surface showed well-defined anodic and cathodic peaks corresponding to the $[Fe(CN)_6]^{3-/4-}$ redox pair. These peaks are overlapped with the redox peaks of the quinone groups of the polymer, are slightly more intense and are displaced 20 mV to lower potentials with respect to GCE/CNOoxi (see Fig. S3c in Supplementary Material), indicating a more favored electron transfer process presumably due to the conjugated character of the polymer and the existence of protonated amino groups at pH 7.4. The immobilization of α-IgA antibodies followed by the blocking step using BSA caused a decrease in the current peaks due to steric hindrance from the immobilized α-IgA and BSA layer. A further decrease in peak currents was observed after incubation with IgA, suggesting the formation of the immunocomplex onto the electrode.

3.2.1. Analytical performance of the IgA immunosensors

The GCE/CNOoxi/poly(L-DOPA/DA)/α − IgA and GCE/poly(L-DOPA/DA)/α − IgA immunosensors were incubated with standard IgA solutions in concentrations ranging from 0 to 5000 ng/mL. In the case of the label-free assay format, the change in the DPV peak current before and after the antigen/antibody immunoreaction (ΔI) was used as analytical output. For the sandwich assay format, the formation of immunocomplex was detected using HRP-labeled anti-IgA conjugate, followed by the measurement of the anodic current produced during the oxidation of TMB.

Fig. 4 shows the calibration plots for IgA detection obtained with

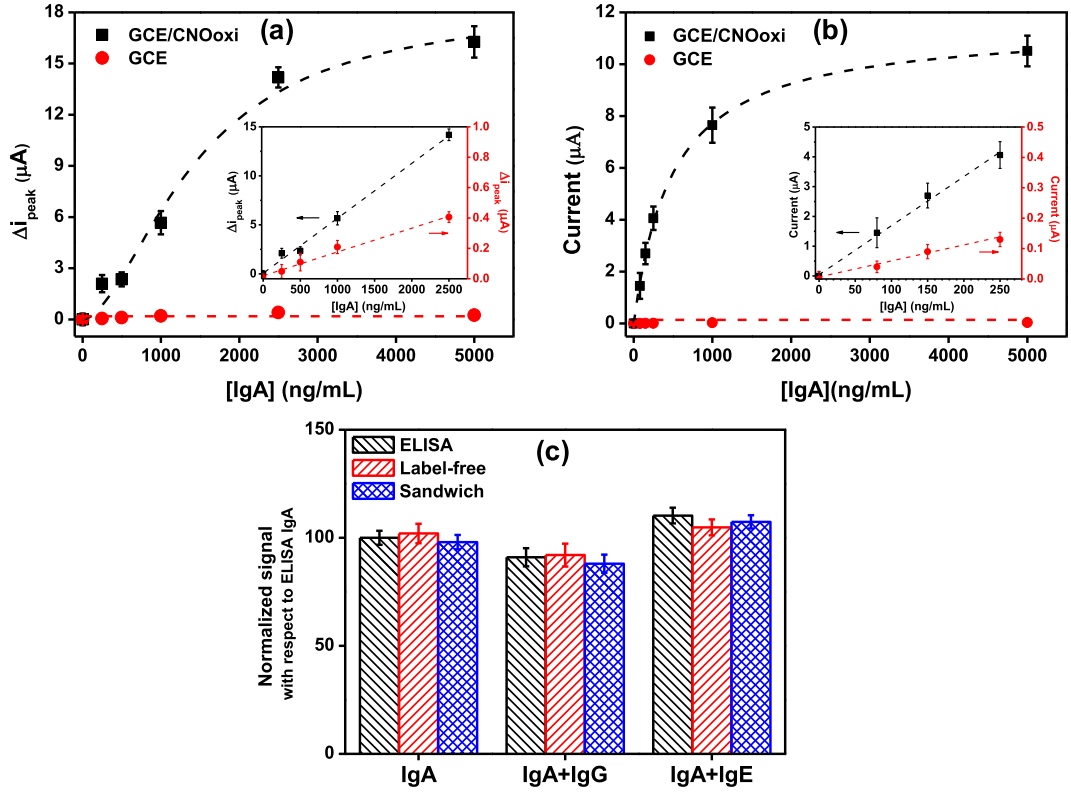

Fig. 4. Calibration curves for IgA obtained with GCE/CNOoxi/poly(L-DOPA/DA)/α-IgA and GCE/poly(L-DOPA/DA)/α-IgA immunosensors using (a) the label-free and (b) the sandwich assay formats. (c) Normalized response of the GCE/CNOoxi/poly(L-DOPA/DA)/α-IgA immunosensor toward 40 ng/mL IgA, 40 ng/mL IgA + 250 ng/mL IgG and 40 ng/mL IgA + 20 ng/mL IgE. Each point is the average of the response obtained with three different biosensors.

Table 1
Comparison of the performance of the presented work with other IgA immunoassays.

Sensing Platform	Signal Source	Method	Linear Range (μg/mL)	LOD (ng/mL)	Assay Time (h)		Reference
					Surface preparation	Detection	
Particle-enhanced nephelometric	ProSpec nephelometer	Nephelometry	4–10.3	450	0	0.2	Booth et al. (2009)
SPE/AuNP-PEG	$[Fe(CN)_6]^{3-/4-}$	SWV	0.087–1	0.5	15	0.75	Rizwan et al. (2018b)
Au/SAM	HRP	Choronoamperometry	0.5–5	170	4	0.5	Rosales-Rivera et al. (2012)
In-house ELISA	HRP	Absorbance	0.0016–0.1	4.2	15	1.25	This work
GCE/CNOoxi/poly(L-DOPA-DA)	$[Fe(CN)_6]^{3-/4-}$	DPV	0–2.5	48	4.5	0.5	This work
	HRP	CV	0–0.25	19	4.5	1.25	

both formats in the presence and in the absence of CNOoxi. A saturation of the immobilized capture antibody takes place at 5000 and 1000 ng/mL of IgA for the label-free and sandwich assays, respectively. For both assay formats, the incorporation of CNOoxi results in a 3-order of magnitude enhancement of the assay sensitivity in comparison with the control surface in the absence of CNOoxi. Assuming a linear behavior between 0–2500 ng/mL IgA, the sensitivity of the label-free biosensor was 5.6 nA ng·mL^{-1}, with a detection limit of 48 ng/mL. In the case of sandwich format, the linear range was up to 250 ng/mL IgA, with a sensitivity of 16.1 nA ng·mL^{-1}and LOD of 19 ng/mL. These values are well below the clinically relevant lower cut-off value for the determination of severe serum IgA immunodeficiencies, which is when the IgA concentration is lower than 70 μg/mL (Thibault et al., 2006). The measurements were also very reproducible, with standard deviations between 7 and 12% for measurements with three different sensors (inter-sensor reproducibility). A comparison between the analytical performances of reported IgA immunosensors with the proposed here is presented in Table 1. Compared with the ELISA assay and other reported sensors using the same immunoreagents, the proposed immunosensors exhibited an excellent sensitivity and linear range.

To monitor the selectivity of the immunosensor, IgG and IgE antibodies that are naturally found in body fluids were investigated for their influence on the IgA detection at the usual concentrations they are found in the serum of healthy individuals. The results were compared with an IgA ELISA assay and are shown in Fig. 4c. IgG resulted in ~8% lower signals while IgE gave slightly increased signals (7%) and in both cases the immunosensor responses to IgA were practically not affected by the presence of the tested interferences with respect to the ELISA assay. Other metabolites such as glucose (5 mM) and ascorbic acid (1 mM) did not interfere in the measurements. Calf serum samples spiked with 70 and 1000 ng/mL of IgA gave signal recoveries of (96 ± 5) and (104 ± 5)% with respect to the value calculated from the calibration curve using the sandwich assay. This indicates that the proposed immunosensors are selective for IgA and are able to work in a complex matrix such as serum with minimal matrix effect.

Finally, storage stability was studied for GCE/CNOoxi/poly(L-

DOPA/DA)/α−IgA biosensors stored in a microarray stabilizer (StabilCoat® Plus) at 4 °C (real time) and 37 °C (under accelerated conditions). After one week, the biosensors stored at 4 °C resulted in essentially the same initial response within the experimental error, while those stored at 37 °C gave 90% of the initial signal. Extrapolating the stability under accelerated conditions to real time using an Arrhenius kinetic model (Laboria et al., 2011), this indicates that the biosensors stored at 4 °C need 39 weeks (~10 months) to decrease their affinity by 10% in this buffer. Therefore, this novel surface chemistry and the storage conditions used preserve antibody affinity facilitating long time storage and is in line with the stabilization observed for enzymes conjugated to CNOs (Sok and Fragoso, 2018).

4. Conclusions

In this work, we have developed a novel electrochemical immunosensor for the detection of IgA antibodies based on the co-electropolymerization of L-DOPA and dopamine on CNOoxi modified glassy carbon electrodes with label-free and sandwich detection. This novel surface provides a surface concentration of reactive carboxylic acid groups comparable to MWCNT-containing three-dimensional matrices, as evidenced by the immobilization of aminoferrocene by amidation reactions. The presence of the CNOs on the electrode surface in combination with the poly-catecholamine thin film increased the sensitivity of the developed electrochemical immunosensors by three orders or magnitude with respect to a poly-catecholamine-only surface. This enhanced sensitivity has been attributed to a combination of high surface area and increased electron transfer rates provided by the CNO layer. The wide linear range and low limits of detection obtained with the two studied immunoassay formats allow the detection of serum IgA in healthy people as well as in IgA deficient patients with the additional advantage of an ease of fabrication and assay simplicity with respect to a classical ELISA assay. These interesting features make the GCE/CNOoxi/poly(L-DOPA/DA) surface a convenient immobilization platform extensible to the analysis of other relevant biomarkers.

Declarations of interest

None.

Declaration of interests

☒ The authors declare that they have no known competing financial interests or personal relationships that could have appeared to influence the work reported in this paper.

CRediT authorship contribution statement

Alex Fragoso: Writing - original draft, Supervision.

Acknowledgments

JCZG thanks the Ministerio de Educación y Formación Profesional (Spain) for a predoctoral scholarship (FPU15/04761). AF thanks financial support from Ministerio de Ciencia, Innovación y Universidades, Spain (grant BIO2017-87946-C2-1-R).

Appendix A. Supplementary data

Supplementary data to this article can be found online at https://doi.org/10.1016/j.bios.2019.111357.

References

Amiri, M., Amali, E., Nematollahzadeh, A., Salehniya, H., 2016. Sensor. Actuator. B Chem. 228, 53–58.
Bahadır, E.B., Sezgintürk, M.K., 2016a. TrAC Trends Anal. Chem. 82, 286–306.
Bahadır, E.B., Sezgintürk, M.K., 2016b. TrAC Trends Anal. Chem. 76, 1–14.
Barclay, T.G., Hegab, H.M., Clarke, S.R., Ginic-Markovic, M., 2017. Adv. Mater. Interfaces 4, 1601192.
Bartolome, J.P., Echegoyen, L., Fragoso, A., 2015. Anal. Chem. 87, 6744–6751.
Bartolome, J.P., Fragoso, A., 2017. Inorg. Chim. Acta 468, 223–231.
Booth, C.K., Dwyer, D.B., Pacque, P.F., Ball, M.J., 2009. Ann. Clin. Biochem. 46, 401–406.
Borgohain, R., Yang, J., Selegue, J.P., Kim, D.Y., 2014. Carbon 66, 272–284.
Clark, M.B., Gardella, J.A., Schultz, T.M., Patil, D.G., Salvati, L., 1990. Anal. Chem. 62, 949–956.
Cruse, J.M., Lewis, R.E., 2010. Atlas of Immunology, third ed. CRC Press, Boca Raton (Chapter 7).
Dai, M., Sun, L., Chao, L., Tan, Y., Fu, Y., Chen, C., Xie, Q., 2015. ACS Appl. Mater. Interfaces 7, 10843–10852.
Diamandis, E.P., Christopoulos, T.K., 1990. Anal. Chem. 62, 1149A–1157A.
Goldsmith, S.J., 1975. Semin. Nucl. Med. 5, 125–152.
Kokkinos, C., Economou, A., Prodromidis, M.I., 2016. TrAC Trends Anal. Chem. 79, 88–105.
Krämer, P., Schmid, R., 1991. Biosens. Bioelectron. 6, 239–243.
Laboria, N., Fragoso, A., O'Sullivan, C.K., 2011. Anal. Lett. 44, 2019–2030.
Le Goff, A., Moggia, F., Debou, N., Jegou, P., Artero, V., Fontecave, M., Jousselme, B., Palacin, S., 2010. J. Electroanal. Chem. 641, 57–63.
Leonardo, S., Toldrà, A., Rambla-Alegre, M., Fernández-Tejedor, M., Andree, K.B., Ferreres, L., Campbell, K., Elliott, C.T., O'Sullivan, C.K., Pazos, Y., Diogène, J., Campàs, M., 2018. Mar. Environ. Res. 133, 6–14.
Liu, Y., Ai, K., Lu, L., 2014. Chem. Rev. 114, 5057–5115.
Mykhailiv, O., Zubyk, H., Plonska-Brzezinska, M.E., 2017. Inorg. Chim. Acta 468, 49–66.
Ortega, G.A., Zuaznabar-Gardona, J.C., Reguera, E., 2018. Biosens. Bioelectron. 116, 30–36.
Pakchin, P.S., Nakhjavani, S.A., Saber, R., Ghanbari, H., Omidi, Y., 2017. TrAC Trends Anal. Chem. 92, 32–41.
Piro, B., Reisberg, S., Piro, B., Reisberg, S., 2017. Recent advances in electrochemical immunosensors. Sensors 17, 794.
Ricci, F., Adornetto, G., Palleschi, G., 2012. Electrochim. Acta 84, 74–83.
Rizwan, M., Elma, S., Lim, S.A., Ahmed, M.U., 2018a. Biosens. Bioelectron. 107, 211–217.
Rizwan, M., Hazmi, M., Lim, S.A., Ahmed, M.U., 2019. J. Electroanal. Chem. 833, 462–470.
Rizwan, M., Koh, D., Booth, M.A., Ahmed, M.U., 2018b. Sensor. Actuator. B Chem. 255, 557–563.
Rosales-Rivera, L.C., Acero-Sánchez, J.L., Lozano-Sánchez, P., Katakis, I., O'Sullivan, C.K., 2012. Biosens. Bioelectron. 33, 134–138.
Sireesha, M., Jagadeesh Babu, V., Kranthi Kiran, A.S., Ramakrishna, S., 2018. Nanocomposites 4, 36–57.
Sok, V., Fragoso, A., 2018. Prep. Biochem. Biotechnol. 48, 136–143.
Soo-Quee Koh, D., Choon-Huat Koh, G., 2007. Occup. Environ. Med. 64, 202–210.
Thibault, L., Beauséjour, A., de Grandmont, M.J., Long, A., Goldman, M., Chevrier, M.-C., 2006. Transfusion 46, 2115–2121.
Trilling, A.K., Beekwilder, J., Zuilhof, H., 2013. Analyst 138, 1619.
Valera, E., Hernández-Albors, A., Marco, M.-P., 2016. TrAC Trends Anal. Chem. 79, 9–22.
Wajs, E., Molina-Ontoria, A., Nielsen, T.T., Echegoyen, L., Fragoso, A., 2015. Langmuir 31, 535–541.
Wild, D., 2013. The Immunoassay Handbook: Theory and Applications of Ligand Binding, ELISA and Related Techniques, fourth ed. Elsevier B.V., Oxford.
Wu, Q., Song, D., Zhang, D., Zhang, H., Ding, Y., Yu, Y., Sun, Y., 2015. Microchim. Acta 182, 1739–1746.
Zhang, P., Guo, X., Wang, H., Sun, Y., Kang, Q., Shen, D., 2017. Sensor. Actuator. B Chem. 248, 551–559.
Zuaznabar-Gardona, J.C., Fragoso, A., 2018. Sensor. Actuator. B Chem. 273, 664–671.